Shugo Takikawa, MD • Vijay Dhawan, PhD • Phoebe Spetsieris, PhD • William Robeson, MSc
Thomas Chaly, PhD • Robert Dahl, PhD • Donald Margouleff, MD • David Eidelberg, MD

Noninvasive Quantitative Fluorodeoxyglucose PET Studies with an Estimated Input Function Derived from a Population-based Arterial Blood Curve[1]

The authors have developed a technique to estimate input functions from a population-based arterial blood curve in positron emission tomography (PET) studies with fluorine-18 fluorodeoxyglucose (FDG). A standardized pump injection was used in 34 subjects. A population-based blood curve was generated based on the first 10 subjects. In the remaining 24 subjects, an estimated input function (EIFa) was obtained by scaling the population-based curve with two arterial blood samples, one obtained at 10 minutes and the other at 45. Time integrals for EIFa and the real arterial input function (RIF) were in excellent agreement ($r = .998$, $P < .0001$). Cerebral metabolic rates for glucose calculated with EIFa and RIF and the autoradiographic method also correlated excellently ($r = .992$, $P < .0001$). Analogous correlations were achieved with arterialized venous samples as scaling factors. These results suggest that individually scaled, population-derived input functions may serve as an adequate alternative to continuous arterial blood sampling in quantitative FDG-PET imaging.

Index terms: Brain, metabolism, 10.12173 • Brain, radionuclide studies, 10.12173 • Emission CT (ECT), 10.12173

Radiology 1993; 188:131–136

POSITRON emission tomography (PET) with fluorine-18 fluorodeoxyglucose (FDG) has been used extensively to investigate regional brain glucose metabolism in conditions of both health and disease. One of the advantages of PET is its ability to accurately quantify physiologic parameters. The three-compartment tracer model originally developed by Sokoloff et al (1) and adapted for PET by Phelps et al (2) can provide quantitative estimation of cerebral glucose metabolic rates (CMRGlc). This model requires an input function that is generally obtained with continuous arterial blood sampling through a catheter placed in the radial artery. However, arterial blood sampling is inconvenient for clinical studies because of the invasive nature of line placement and the time and staff needed for the collection and processing of the samples (3).

Several attempts have been made to develop a substitution for arterial blood sampling to obtain an input function. Arterialized venous blood sampling from a heated venous line has been accepted as an alternative to arterial sampling in the FDG study (2,4). This method can make the procedure less invasive but does not resolve the inconvenience associated with the processing of numerous blood samples. Dynamic monitoring of radioactivity from the cardiac blood pool (5,6), the abdominal aorta (7,8), and the radial artery (9) has been employed to acquire usable noninvasive input functions. All of these techniques require dynamic scanning with a whole-body tomograph or a second small-diameter tomograph dedicated to a peripheral artery, as well as extra time for analyzing dynamic images. Moreover, a large number of short time-duration scans are associated with increased digital storage requirements. As a simple alternative to these procedures, we developed a technique to estimate the FDG input function from a population-based arterial blood curve. The purpose of this study was to validate this new method by testing the accuracy of the estimated input function and comparing the CMRGlc values calculated with it versus those calculated with the actual arterial blood curve.

MATERIALS AND METHODS

Subjects and PET Procedure

The study consisted of 34 subjects (21 men and 13 women; mean age, 49 years ± 17; range, 23–76 years), 13 healthy volunteers and 21 patients with a movement disorder. All 34 individuals underwent imaging with use of a Super PETT-3,000 time-of-flight camera (Scanditronix, Essex, Mass) (in-plane reconstructed resolution is 10 mm full width half maximum, and axial resolution is 6–10 mm). The performance characteristics of this instrument have been described elsewhere (10,11). All studies were performed after the subject fasted overnight in a resting condition defined by a dimly lit PET suite and minimal auditory stimulation (both ears and eyes open). Head position was maintained throughout the scanning procedure with a polyurethane custom head mold (12).

After 15 minutes of transmission scanning for attenuation correction with a germanium-68 sector source, 14.8–37 × 10^{10} Bq of FDG (approximately 0.37 × 10^{10} Bq/kg) in 4.0 mL of saline solution was injected into an antecubital vein with an infusion pump at a standard rate (6.0 mL/min). The transit time from injection point to the brain (brain delay) was measured with the coincidence counter on the scanner, that is, the time point at which three consecutive increases of count are ob-

[1] From the Departments of Neurology (S.T., V.D., P.S., D.E.) and Medicine (W.R., T.C., R.D., D.M.), North Shore University Hospital–Cornell University Medical College, 300 Community Dr, Manhasset, NY 11030. From the 1992 RSNA scientific assembly. Received November 2, 1992; revision requested December 31; revision received January 25, 1993; accepted February 16. Supported by grants from the Parkinson Disease Foundation and the Dystonia Medical Research Foundation. **Address reprint requests to** D.E.

Abbreviations: AUC = area under the curve, CMRGlc = cerebral glucose metabolic rate, EIFa = estimated input function scaled by arterial samples, EIFv = estimated input function scaled by arterialized venous samples, FDG = fluorodeoxyglucose, GMR = global metabolic rate, PET = positron emission tomography, RIF = real input function determined by continuous arterial sampling, ROI = region of interest.

served. In cases in which a dynamic estimation of kinetic rate constants was necessary, scanning was started simultaneously with the initiation of the injection. Continuous scanning data were collected for 35 minutes in list mode, and images were reconstructed with a spatial resolution of 10 mm at the following time frames: six scans of 0.5-minute duration, two scans of 1 minute, five scans of 2 minutes, followed by five scans of 4 minutes. Final "autoradiographic" brain images were acquired for 20 minutes beginning 35 minutes after the injection was initiated. Concurrent with an injection of FDG, arterial blood samples were obtained through a catheter placed in the radial artery with a precision peristaltic pump for the first 16 samples at every 9 seconds, followed by manual sampling at 3.5, 5, 7, 10, 15, 20, 30, 45, and 55 minutes after injection. In 11 cases, arterialized venous blood was also drawn from the vein of a hand heated to 44°C in a small warm-air chamber. Samples were immediately placed on ice and subsequently centrifuged to separate plasma for the determination of plasma FDG concentrations with a multi-channel analyzer. FDG activity in each sample was represented as a ratio by dividing it by Ge-68 activity in a calibration tube. Because the first 16 arterial samples were collected with a pump, an appropriate smearing correction was applied (13). Plasma glucose concentration was obtained from three samples acquired at 0, 30, and 45 minutes after injection.

Ethical permission for these studies was obtained from the Institutional Review Board of North Shore University Hospital–Cornell University Medical College. Written consent from all subjects was obtained after a detailed explanation of the scanning procedure.

Population-based Arterial Blood Curve and Estimated Input Function

A population-based arterial blood curve was generated by averaging the actual arterial blood curves obtained from the first 10 subjects (three healthy subjects and seven patients, seven men and three women; mean age, 49 years ± 17; range, 23–76 years; mean body weight, 70 kg ± 15; range, 46–93 kg; mean height, 175 cm ± 11; range, 160–188 cm). Before averaging, the amplitude of each blood curve was normalized to a standard 0.37×10^{10} Bq/kg injection, and its time scale was corrected for the transit time from injection point to the sampling site (blood delay). At each time point (for the population-based curve), activities of individual-based blood curves were determined with linear interpolation if necessary and then averaged to obtain the final activities for the population-based curve.

In each of the remaining 24 subjects (10 healthy subjects and 14 patients, 14 men and 10 women; mean age, 49 years ± 17; range, 23–73 years; mean body weight, 69 kg ± 14; range, 45–91 kg; mean height, 174 cm ± 13; range, 150–190 cm), the estimated input function was obtained by scaling the population-based curve with the individual's actual arterial blood activity. In this study, we limited the number of the blood samples used for scaling to one or two to simplify the procedure as much as possible. To determine the timing of the most appropriate sample or pair of samples for scaling the population-based curve, we correlated the activity of the individual arterial samples with the time integral (area under the curve [AUC]) of the individual's own arterial blood curve. In 34 subjects, we measured the AUC of the blood curve between 0 and 45 minutes after injection by using a simple trapezoidal algorithm and the activity in various single samples and the mean activity in various sample pairs. We then identified the single or paired samples that best predicted the AUC of the blood curve and used the activity measured at these time points to scale the population-based curve in subsequent cases. We defined the estimated input function as follows:

$$Ce(t) = Cp(t - \delta) \times \frac{\overline{A_{ij}}}{\overline{C_{ij}}},$$

where

$$\overline{A_{ij}} = \frac{A_i + A_j}{2} \quad \text{and}$$

$$\overline{C_{ij}} = \frac{Cp(i - \delta) + Cp(j - \delta)}{2},$$

where $Ce(t)$ = estimated input function, $Cp(t)$ = population-based arterial blood curve, δ = estimated blood delay (minutes) that was obtained by adding 17 seconds (an average lag time between brain delay and blood delay in our standardized injection) to the actual measured brain delay, i and j = time points (minutes after injection) at which the blood samples for scaling are drawn (i is not equal to j for a pair of samples but is equal for a single sample), and Ai and Aj = the FDG activity of these samples.

To assess the comparability of arterialized venous sampling to arterial sampling in our method, we scaled the population-based blood curve by using arterialized venous samples and arterial samples according to the first equation in 11 of 24 subjects whose data were not used to generate the population-based curve.

Image Processing

Glucose metabolic rate.—All image processing such as transformation of raw count images into parametric images ("functionalization") and region of interest (ROI) analysis were performed on a microcomputer (SPARC Server 490; SUN Microsystems, Mountain View, Calif) and Scan V/P Software developed in our laboratory (14). CMRGlc values were calculated with the autoradiographic method developed by Sokoloff et al (1) and adapted for PET by Phelps et al (2). We employed a population-based mean gray matter rate constant ($k_1 = 0.1112$, $k_2 = 0.1649$, $k_3 = 0.1122$) calculated by us previously in 12 healthy control subjects; k_4 was fixed at 0.0068 (15). A value of 0.42 was used for the lumped constant (2). In each subject, functionalization into the CMRGlc image was accomplished with two or three input functions: (*a*) a real input function determined by continuous arterial sampling (RIF), (*b*) the estimated input function scaled by arterial samples (EIFa), and (*c*) the estimated input function scaled by arterialized venous samples (EIFv). A large ROI was positioned to encompass all gray matter on a single PET section containing the basal ganglia. The top 20th percentile of functionalized ROI pixels was selected for the calculation of the global metabolic rate (GMR) for glucose (16). A standardized ROI ($n = 12$; lateral and medial frontal, superior temporal, occipital, thalamic, and basal ganglionic regions in each hemisphere) was additionally drawn on the same plane; normalized regional CMRGlc values defined as a ratio of regional CMRGlc to GMR were calculated for each ROI. In each subject, ROI coordinates were spatially fixed on the parametric images derived from the various input functions.

Kinetic rate constants.—In seven of 24 subjects who underwent dynamic and autoradiographic PET scanning, gray matter kinetic rate constants were calculated with two input functions, RIF and EIFa. The time course of brain radioactivity was measured in the same large ROI as that used in the autoradiographic GMR calculations. The uptake curve was fitted, allowing for three rate constants ($k_1 - k_3$) and cerebral blood volume; k_4 was fixed at 0.0068 (15,17). Estimated values of $k_1 - k_3$ were then used to calculate dynamic estimates of GMR based on individual rate constants according to the following equation (4): $CMRGlc = Cglc / LC \times k_1k_3 / (k_2 + k_3)$, where $Cglc$ = plasma glucose concentration, and LC = lumped constant assumed at 0.42.

Statistics.—We used correlation analysis (Pearson product moment) to compare the AUC of EIFa and EIFv and resulting CMRGlc values (GMR and normalized regional CMRGlc) with the corresponding values obtained with RIF. The differences in these correlations between healthy subjects and patients were also examined with a z test. Additionally, we compared dynamic estimates of $k_1 - k_3$ and dynamic GMR derived from EIFa with corresponding estimates derived from RIF.

RESULTS

Correlation between Individual Sample Activity and the AUC

The correlation coefficients of the activity of each arterial blood sample and the mean activity of various paired samples with the AUC of the arterial blood curves ($n = 34$ subjects) are presented in Table 1. The activity of each individual blood sample cor-

Table 1
Correlation Coefficients of Plasma Activities at Various Times after Injection with the AUC

A_j A_i	A_{peak}	A_5	A_7	A_{10}	A_{15}	A_{20}	A_{30}	A_{45}
A_{peak}	*.884*	.925	.922	.915	.915	.914	.908	.904
A_5		*.983*	.988	.990	.993	.994	.995	.995
A_7			*.989*	.992	.995	.995	.996	.996
A_{10}				*.989*	.995	.996	.996	.997
A_{15}					*.995*	.995	.996	.995
A_{20}						.993	.994	.992
A_{30}							*.988*	.987
A_{45}								*.982*

Note.—Values along the diagonal (italicized) represent the correlation coefficients between the activities of individual samples obtained at time *i* after injection (A_i), with the AUC from 0 to 45 minutes. Values above the diagonal represent the correlation coefficients between the AUC and the mean activities of pairs of individual samples obtained at various defined time points (A_{ij}). For instance, $A_{10,45}$ represents the mean value of the individual activities at 10 and at 45 minutes after injection. $A_{10,45}$ correlates closely with the AUC (r = .997), yielding the most suitable activity for scaling of those examined. A_{peak}, the activity at the peak of the arterial blood curve, was the least well correlated with the AUC.

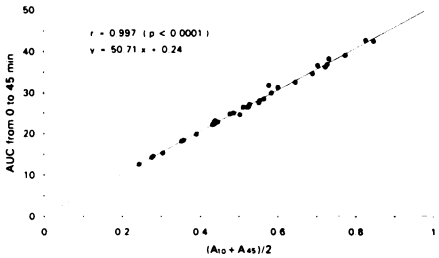

Figure 1. Graph shows the correlation between the mean value of arterial FDG activities at 10 and at 45 minutes after injection (A_{10} and A_{45}) and the AUC from 0 to 45 minutes for 34 FDG-PET studies.

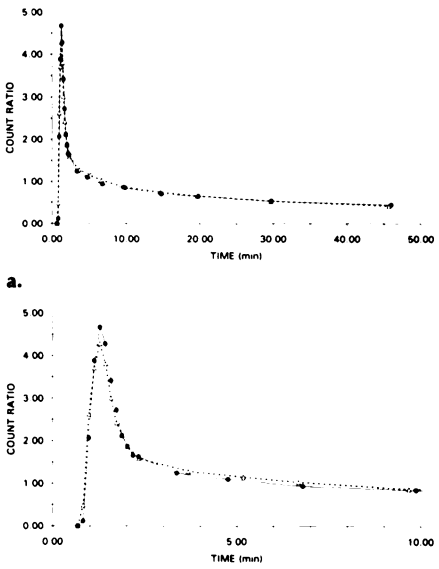

Figure 2. **(a)** Graph shows the RIF (● with solid line) and EIFa with two arterial samples at 10 and at 45 minutes after injection (△ with dashed line) in a representative case. **(b)** Graph shows the expanded peak region.

related variably with the AUC. The best correlation coefficient with the AUC was provided by the mean activity of individual samples obtained at 10 and 45 minutes after injection (r = .997; Fig 1). In addition to the highly significant correlation, the y intercept (0.24) of this regression line was negligible compared with the magnitude of the AUC. Therefore, the AUC was considered to be virtually proportional to the mean activity of these two samples. On the basis of this result, we selected the 10- and 45-minute samples for scaling the population-based curve to obtain EIFa and EIFv according to the first equation.

Comparison between EIFa and RIF

EIFa was compared with RIF in the range from t = 0 minute (injection time) to t = 45 minutes (middle of the scanning time for an autoradiographic image), which is usually necessary to calculate CMRGlc. Each pair of input functions showed good agreement in shape and magnitude, except for the variation in the peak height and in the shape of the "knee" portion (ie, the portion that intervenes between the rapid and the slow washout phases, usually 3–10 minutes after injection) (Fig 2). A summary of quantitative comparison is shown in Table 2. Blood delay and peak time could be estimated precisely. Peak heights for estimated and real curves differed by 3.4% ± 14.2% in their averages. The mean percentage of difference in the AUC from 0 to 45 minutes was very small (0.3% ± 1.7%), with a maximum difference of less than 4%. Linear regression analysis for the AUC demonstrated excellent agreement between EIFa and RIF, with a slope equal to one (r = .998, P < .0001, slope = 1.000 ± 0.012; Fig 3).

GMR estimates based on EIFa and RIF were also compared. The mean percentage of difference in GMR measured with EIFa and RIF was 0.9% ± 2.5%, with a maximum difference of 4.4%. Linear regression analysis for the two GMR estimates again revealed excellent agreement (r = .992, P < .0001, slope = 0.983 ± 0.026; Fig 4). The differences in GMR measured with EIFa and RIF correlated significantly with the AUC differences in the two input functions (r = −.731, P < .001; Fig 5). Normalized regional CMRGlc values based on the two input functions were compared in each ROI. Agreement between these values was similar in each ROI (mean r value, .999 ± .0001; mean P value < .0001; mean slope of regression lines, 0.991 ± 0.012), suggesting that normalized regional CMRGlc values derived from EIFa and RIF are virtually identical. An example of the linear regressions for normalized regional CMRGlc values is given in Figure 6.

Correlation between the AUC of EIFa and RIF in 10 healthy subjects (r = .998, P < .0001, slope = 1.009 ± 0.023) was not significantly different (P > .6) from that in 14 patients (r = .997, P < .0001, slope = 1.001 ± 0.023). No significant difference (P > .2) in the GMR correlation was found between the two groups (r = .985, P < .0001, slope = 1.054 ± 0.067 for the healthy group; r = .995, P < .0001, slope = 1.048 ± 0.031 for the patient group). In addition, although the plasma glucose concentration was within normal range in all subjects (80–112 mg/dL), no correlation was shown between plasma glucose levels and differences in the AUC of the two input functions (r = .05) or between plasma glucose levels and differences in the GMR (r = .10), suggesting that agreement between EIFa and RIF is not dependent on plasma glucose concentration.

Comparison of kinetic rate constants in dynamic FDG-PET studies with EIFa and RIF as input functions revealed substantial differences in estimated rate constants (Table 3).

Table 2
Differences between Parameters of EIF_a (Two Samples) and RIF

	Blood Delay	Peak Time	Peak Height*	AUC*	GMR*	Normalized rCMRGlc*
Mean ± SD	0 sec ± 5	1 sec ± 7	3.4% ± 14.2%	0.3% ± 1.2%	0.9% ± 2.5%	0% ± 0.2%
Maximum difference	18 sec	18 sec	33.6%	3.8%	4.4%	1.1%

Note.—rCMRGlc = regional CMRGlc, SD = standard deviation.
* Differences are expressed as [(estimate − real)/real] × 100%. The AUC is from 0 to 45 minutes. The GMR is for glucose. Normalized rCMRGlc is per GMR.

However, dynamic estimates of GMR determined with these two sets of rate constants were still in good agreement between EIFa and RIF ($r = .985$, $P < .0001$).

Comparison between EIFv and RIF

Table 4 shows the mean and standard deviation of the ratios of arterialized venous to arterial FDG counts and the ratios of arterialized venous to arterial plasma glucose concentration at 10 and at 45 minutes after injection. With these differences between arterialized venous and arterial samples, we examined whether EIFv and RIF can have as good agreement as EIFa and RIF. The mean percentage of differences in the AUC and GMR values between EIFv and RIF were slightly larger than those between EIFa and RIF (Table 5). Linear regression analysis, however, again demonstrated excellent agreement between EIFv- and RIF-derived parameters, as follows: (*a*) $r = .998$, $P < .0001$, slope = 0.968 ± 0.021 for AUC; (*b*) $r = .989$, $P < .0001$, slope = 0.952 ± 0.047 for GMR; and (*c*) mean r value in 12 ROIs = .999 (±.001), mean P value in 12 ROIs was < .0001, mean slope in 12 ROIs = 0.993 (±0.021) for normalized regional CMRGlc values. These results were comparable to those between EIFa and RIF, which indicates an agreement between arterial and arterialized venous samples as scaling factors for the population-based blood curve.

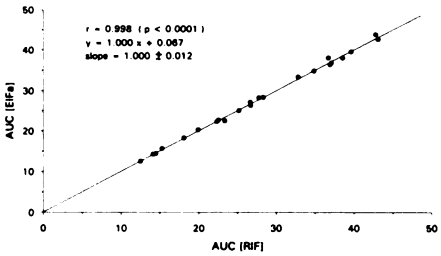

3.

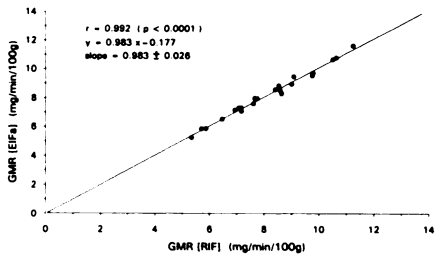

4.

Figures 3, 4. **(3)** Graph shows the correlation between the time integrals (*AUC*) from 0 to 45 minutes of RIF and EIF_a (two samples) for 24 FDG-PET studies. **(4)** Graph shows the correlation between the GMR for glucose values derived from the two input functions (RIF and EIFa [two samples]) and the autoradiographic method in 24 FDG-PET studies.

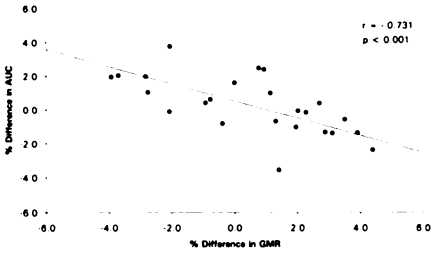

5.

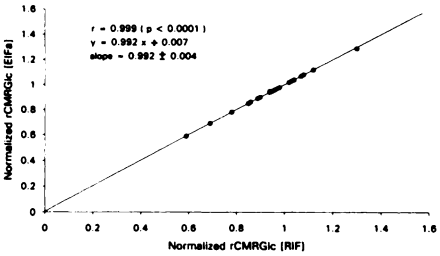

6.

Figures 5, 6. **(5)** Graph shows the correlation between the percentage of differences in GMR for glucose and time integral (*AUC*) measured with the two input functions (RIF and EIFa [two samples]) for 24 FDG-PET studies. **(6)** Graph shows the correlation between the normalized regional CMRGlc (*rCMRGlc*) values in the left basal ganglia based on RIF and EIFa (two samples) for 24 FDG-PET studies.

DISCUSSION

With greater numbers of clinical PET studies performed currently (18), it has become desirable to develop simple and less invasive procedures for quantitation (3). As an alternative to frequent arterial blood sampling in FDG-PET studies, we report a new technique to estimate the input function by scaling a population-derived blood curve by using only two blood samples.

Input function for bolus FDG administration depends on various individual factors such as physical measurements, cardiovascular state, and renal function, as well as injection-related variables such as dose, volume, speed, and site. Although the injection-related variables can be standardized, it is difficult to standardize the individual factors affecting the input function. Nonetheless, the composite effect of these factors is reflected in the FDG activity of each blood sample and may be accounted for to some degree by scaling a standard blood curve (derived from a population-based average for a well-defined injection protocol) by the plasma FDG activity measured in a limited number of samples obtained from the individual subject.

Fortunately, unlike the dynamic estimates of regional rate constants, the autoradiographic method for CMRGlc estimation has an advantage of less sensitivity to errors in the measurement of the input function (19), and calculated CMRGlc values are primarily dependent on the time integral of input function instead of its rate of change, as shown in the operational equation of Rhodes et al (20). Thus, the most crucial issue is the number and timing of the individual blood samples needed for scaling the population-based curve to obtain the estimated input function that best predicts the time integral for the real arterial blood curve.

To answer this question, we examined the correlation between the activity of the individual samples singly or as the average of two samples and the time integral of the blood curves. We found that the mean activity of the 10- and 45-minute samples correlated most closely and was proportional to the time integral. This suggests that these two samples may be the optimal pair to scale the population-based curve that has a fixed

Table 3
Differences in Kinetic Rate Constants and Resulting Metabolic Rates with EIFa (Two Samples) and RIF

Case	Percentage of Difference*			
	k_1 (%)	k_2 (%)	k_3 (%)	GMRd (%)
1	9.2	27.8	6.1	−1.0
2	−3.5	−6.3	4.8	2.9
3	24.7	59.9	11.5	0.6
4	14.9	37.9	11.4	2.5
5	4.0	6.7	5.7	3.5
6	−12.0	−17.3	2.2	0.3
7	4.0	6.7	5.7	3.5
Mean	5.9	16.5	6.8	1.8
SD	12.0	26.8	3.4	1.8

Note.—GMRd = dynamic GMR, SD = standard deviation.
* Differences are expressed as [(estimate − real)/real] × 100%. GMRd for glucose was calculated with the dynamic images obtained with 0–35-minute and individual rate constants.

Table 4
Arterialized Venous to Arterial Ratio (V/A) of Plasma FDG and Glucose Concentration

V/A (FDG)			V/A (Glc)	V/A (Glc)/V/A (FDG)
10 min	45 min	Average	Average	Average
0.97 ± 0.03	1.03 ± 0.02	0.99 ± 0.02	0.97 ± 0.02	0.98 ± 0.02

Note.—All values are expressed as mean ± standard deviation. Glc = glucose.

Table 5
Differences between Parameters of EIFv and RIF

	AUC	GMR	Normalized rCMRGlc
Mean ± SD	−0.8% ± 2.7%	−1.0% ± 2.7%	0% ± 0.2%
Maximum difference	−5.2%	−5.2%	1.4%

Note.—Differences are expressed as [(estimate − real)/real] × 100%. rCMRGlc = regional CMRGlc, SD = standard deviation. The AUC is from 0 to 45 minutes. GMR is for glucose. Normalized rCMRGlc is per GMR.

value of time integral. In fact, it was confirmed that the estimated input functions scaled by these two samples were in excellent agreement with the actual arterial blood curve, not only in their time integrals but also in GMR values determined by using them. This result supports our premise that GMR values are virtually dependent on the AUC of input functions and validates indirectly the use of the AUC to select the time points for scaling. However, because we used the modified method of Phelps et al (2) for GMR calculations instead of the method of Rhodes et al (20), calculated GMR values were influenced by the temporal shape of the input function to a small extent, in addition to the primary dependence on the AUC of the input function. For this reason, the correlation between differences in GMR and differences in AUC was significant but not perfect. Individual curves have slightly different temporal behavior compared with that of the population-based curve. Therefore, similar differences in the AUC between individuals could result from differences occurring at various time periods, resulting in less ideal correlation between differences in the AUC (not the AUC) and differences in GMR (not GMR), as shown in Figure 5. Another reason for using the AUC to select the time points for scaling the population-based curve is that the AUC is the most direct comparison of input functions available. On the other hand, GMR cannot be used for the same purpose because the calculation of GMR involves not only the input function but also plasma glucose level and brain activity data that include their own measurement errors.

We used 10- and 45-minute samples to scale the population-based curve in this study because the mean activity of these values provided the highest correlation coefficient with the AUC of those examined, even though correlations of other pairs with the AUC were nearly as good as this value. This combination of two samples is, therefore, not exclusive. Other sample pairs or single samples with a high correlation to the time integral may also provide adequate input function estimations. For instance, we found that EIFa scaled by the activity of a 15-minute arterial sample, whose activity yielded the highest correlation coefficient ($r = .995$) with the AUC in all single samples in Table 1, produced good agreement with RIF in the AUC ($r = .997$, $P < .0001$). However, the differences in the AUC of the two input functions were larger (mean percentage of difference, −1.2% ± 2.7%; maximum percentage of difference, −6.7%) than those we reported above with two samples for scaling. Conversely, additional blood sampling for scaling may provide even better predictions of RIF, although more than two samples appear to be unnecessary.

Our data indicate that the population-based estimated input function can provide accurate estimates of CMRGlc in the autoradiographic method with population-based mean rate constants. However, as shown in Table 3, this estimated input function cannot be used as an alternative to the actual arterial input function in the calculation of individual kinetic rate constants with dynamic PET. Because, by definition, all estimated input functions have the same rate of change, such functions are not adequate for kinetic calculations in which their rate of change and total amount of FDG delivered are equally important (21). It is, however, interesting to note that despite substantial differences in estimates of each rate constant, the individual value of $k_1k_3/(k_2 + k_3)$ was predicted closely with EIFa, yielding a good agreement in resulting dynamic GMR values between EIFa and RIF.

Arterialized blood sampling from a heated venous line has been accepted as an alternative to arterial blood sampling in FDG-PET studies since Phelps et al (2) reported the similarity between the results of the two methods. By using arterialized venous samples and our new technique, the blood sampling method is simplified to only two venous samples from a heated hand. It was noted that an arterialized venous time-activity curve has problems of a delayed and broadened peak as compared with an arte-

rial time-activity curve (21). However, these physical problems associated with the arterialized venous blood method appear to be less important in our method because the activity differences between arterial and arterialized venous blood are relatively smaller at our sampling points. Our limited data from 11 patients suggest a close agreement between arterial and arterialized venous samples as scaling factors for the population-based blood curve, yielding equivalently accurate predictions of RIF and resulting CMRGlc.

Individually scaled population-derived input functions are a useful alternative to continuous blood sampling in quantitative FDG-PET studies. This simple technique may substantially reduce patient discomfort and risk while minimizing both processing time and personnel exposure to blood samples. However, it should be remembered that this procedure has been validated only for the autoradiographic method in FDG-PET studies. Further studies are necessary to validate the application of this technique to subjects with an altered glucose balance (eg, in diabetes mellitus, glucose loading state, or insulin clamping), as well as to subjects with extremes of body surface dimensions such as small children or individuals with morbid obesity.

CONCLUSIONS

The input function for FDG-PET studies can be accurately estimated with a population-derived blood curve scaled with two arterial or arterialized venous blood samples. The advantages of simplicity and limited invasiveness make this technique applicable to clinical studies performed with both brain and whole-body PET scanners. This technique predicts CMRGlc values with sufficient accuracy to be applied in a research setting. ■

Acknowledgments: The authors thank Janie Dill for help with the PET studies; Abdel Belakhlef, PhD, and Ralph Mattachieri for cyclotron support, and Dibyendu Bandyopadhyay, PhD, for radiochemistry assistance.

References

1. Sokoloff L, Reivich M, Kennedy C, et al. The [^{14}C] deoxyglucose method for the measurement of local cerebral glucose metabolism: theory, procedure and normal values in the conscious and anesthetized albino rat. J Neurochem 1977; 28:897–916.
2. Phelps ME, Huang SC, Hoffman EJ, Selin C, Sokoloff L, Kuhl DE. Tomographic measurement of local cerebral glucose metabolic rate in humans with (^{18}F) 2-fluoro-2-deoxy-D-glucose: validation of method. Ann Neurol 1979; 6:371–388.
3. Correia J. A bloody future for clinical PET? (editorial). J Nucl Med 1992; 32:620–622.
4. Huang SC, Phelps ME, Hoffman EJ, Sideris K, Selin CJ, Kuhl DE. Noninvasive determination of local cerebral metabolic rate of glucose in man. Am J Physiol 1980; 238: E69–E82.
5. Weinberg IN, Huang SC, Hoffman EJ, et al. Validation of PET-acquired input functions for cardiac studies. J Nucl Med 1988; 29: 241–247.
6. Gambhir SS, Schwaiger M, Huang SC, et al. Simple noninvasive quantification method for measuring myocardial glucose utilization in humans employing positron emission tomography and fluorine-18 deoxyglucose. J Nucl Med 1989; 30:359–366.
7. Dhawan V, Takikawa S, Robeson W, et al. Fully quantitative neurological FDG/PET studies without arterial blood sampling (abstr). J Nucl Med 1992; 33:922.
8. Germano G, Chen BC, Huang SC, Gambhir SS, Hoffman EJ, Phelps ME. Use of the abdominal aorta for arterial input function determination in hepatic and renal PET studies. J Nucl Med 1992; 33:613–620.
9. Rajeswaran S, Biley DL, Jones T, et al. 2-D and 3-D imaging of small animals and the human radial artery with a high resolution detector for PET. IEEE Trans Med Imaging 1992; 11:386–391.
10. Robeson W, Dhawan V, Babchyck B. A new approach to the measurement of resolution and sampling on a positron emission tomograph. IEEE Trans Nucl Sci 1990; 37: 1506–1513.
11. Robeson W, Dhawan V, Takikawa S, et al. SuperPETT 3000 time-of-flight tomograph: optimization of factors affecting quantification. IEEE Trans Nucl Sci 1993; 40:135–142.
12. Dhawan V, Jarden JO, Strother S, Rottenberg DA. Effect of blood curve smearing on the accuracy of parameter estimates obtained for 82Rb/PET studies of blood-brain barrier permeability. Phys Med Biol 1988; 33:61–74.
13. Kearfott KJ, Rottenberg DA, Knowles RJR. A new headholder for PET, CT and NMR imaging. J Comput Assist Tomogr 1984; 8:1217–1220.
14. Spetsieris P, Dhawan V, Takikawa S, Margouleff D, Eidelberg D. A versatile graphics-image processing package for imaging cerebral function. IEEE CG&A 1993; 13:15–26.
15. Dhawan V, Moeller JR, Strother SC, Evans AC, Rottenberg DA. Effect of selecting a fixed dephosphorylation rate on the estimation of rate constants and rCMRGlc from dynamic [^{18}F]fluorodeoxyglucose/PET data. J Nucl Med 1989; 30:1483–1488.
16. Rottenberg DA, Moeller JR, Strother SC, Dhawan V, Sergi ML. Effects of percent thresholding on the extraction of [^{18}F]fluorodeoxyglucose positron emission tomographic region-of-interest data. J Cereb Blood Flow Metab 1991; 11(suppl):A83–A88.
17. Evans AC, Diksic M, Yamamoto YL, et al. Effect of vascular activity in the determination of rate constants for the uptake of 18F-labeled 2-fluoro-2-deoxy-D-glucose: error analysis and normal values in older subjects. J Cereb Blood Flow Metab 1986; 6: 724–738.
18. Wagner HN. Clinical PET: its time has come (commentary). J Nucl Med 1991; 32: 561–564.
19. Clark CM, Grochowski EW, Ammann W. A method for comparing different procedures of estimating regional glucose metabolism using fluorine-18-fluorodeoxyglucose. J Nucl Med 1992; 33:157–160.
20. Rhodes CG, Wise RJS, Gibbs JM, et al. In vivo disturbance of the oxidative metabolism of glucose in human cerebral gliomas. Ann Neurol 1983; 14:614–626.
21. Budinger TF, Huesman RH, Knittel B, Friedland RP, Derenzo SE. Physiological modeling of dynamic measurements of metabolism using positron emission tomography. In: Greitz T, ed. The metabolism of human brain studied with positron emission tomography. New York, NY: Raven, 1985; 165–183.